energies

Article

Levelized Cost of Heat of the CSP_{th} Hybrid Central Tower Technology

Irving Cruz-Robles, Jorge M. Islas-Samperio and Claudio A. Estrada *

Institute of Renewable Energy, National Autonomous University of Mexico (IER-UNAM), Priv. Xochicalco S/N, Temixco 62580, Morelos, Mexico
* Correspondence: cestrada@ier.unam.mx

Abstract: Process heating represents about two-thirds of the energy that the industry sector consumes worldwide; this energy comes primarily from burning fossil fuels. There is a wide variety of processes for which solar technologies can supply energy. Within these technologies, the CSP_{th} Central Tower produces heat at temperatures about 600 °C, making it suitable for high-temperature processes. A CSP_{th} Central Tower can be combined with a fuel-based system to form a CSP_{th} Hybrid Central Tower system, which results in a high-reliable energy source with low rates of CO_2 emissions. In this work, the levelized cost of heat (*LCOH*) of the CSP_{th} Hybrid Central Tower technology was calculated. SolarPILOT was used to design and evaluate the CSP_{th} Central Tower; fuel consumption was calculated using a steady-state energy balance. The *LCOH* was evaluated considering the CO_2 prices recommended by the High-Level Commission on Carbon Pricing. The analysis shows that this technology can be highly competitive and, in certain cases, shows lower *LCOH* than fuel-based systems. However, these cases depend on reasonable CO_2 prices, low costs of capital (≈5%), and efforts to reduce the capital expenditure, which can nowadays be possible for CSP_{th} Hybrid Central Tower systems designed with large solar multiples.

Keywords: CSP_{th} Central Tower technology; industrial process heating; levelized cost of heat

check for updates

Citation: Cruz-Robles, I.; Islas-Samperio, J.M.; Estrada, C.A. Levelized Cost of Heat of the CSP_{th} Hybrid Central Tower Technology. *Energies* **2022**, *15*, 8528. https://doi.org/10.3390/en15228528

Academic Editor: Donato Morea

Received: 13 October 2022
Accepted: 8 November 2022
Published: 15 November 2022

1. Introduction

Energy is an important input for all kinds of activities; however, energy consumption is highly correlated with greenhouse gas emissions: in 2018, the annual energy-related CO_2 emissions reached 33.1 Gt of CO_2 [1]. In the same year, the industry sector participated with 29% of the world's energy consumption [2]. Process heating represents about two-thirds of the energy that the industry uses [3], this energy comes primarily from burning fossil fuels, meanwhile renewable energy covers just 10% of this heat demand [4]. Burning fossil fuels also leads to price instabilities, shortages, and political conflicts. As industrial production will increase by a factor of four by 2050 [5], there is a great interest to deploy renewable technologies for industrial process heating.

Industrial processes can be classified into three temperature levels: low (<100 °C), medium (100–400 °C), and high (>400 °C) temperature processes [6]. There are several studies about using non-concentrating and concentrating solar thermal technologies for process heat supply. Examples of such applications are found in sectors like the dairy industry [7,8], district heating [9], textile industry [10,11], food industry [12,13], and pharmaceutical industry [14]. Nowadays, several solar thermal systems provide heat to a large variety of industrial processes [15–18].

Implementation of solar thermal systems requires both technical and economic assessments. Whereas the technical evaluation can be carried out using a specialized software, the economic evaluation can be carried out through several techniques: common techniques include the payback period (PB), the net present value (NPV), and the internal rate of return (IRR); however, a better framework to express the cost of producing heat is the levelized cost of heat (*LCOH*) [19].

The *LCOH* has been used to analyze low-temperature solar thermal technologies [20] and medium-temperature solar thermal technologies [21–24]. Nevertheless, these technologies provide heat at temperatures below 350 °C. High-temperature processes and heat loads greater than 10 MW_{th} are potential opportunities for alternative energy sources [25].

At the current commercial state, the Concentrating Solar Power (CSP) Central Tower technology produces heat at temperatures above 600 °C and can be scaled in the order of megawatts. Furthermore, CSP systems provide a high-reliable energy supply if combined with fuel-based systems: this combination is known as CSP Hybrid systems [26]. It should be noted that "CSP" refers to electric power generation; for this work, the term CSP_{th} was introduced to refer to Concentrating Solar Thermal Power. The above-mentioned characteristics make CSP_{th} Hybrid Central Tower systems (CSP_{th} Hybrid-CT systems) a promising technology for delivering high-temperature heat to high-temperature industrial processes.

In this context, CSP_{th} Hybrid-CT systems have been studied before for the ammonia production process [27]; however, in that work the economic parameter was the ammonia generation cost instead of the *LCOH*. These kinds of economic parameters make it difficult for other industries to visualize the economic potential of using this technology for their processes. On the other hand, studies about the *LCOH* of the CSP_{th} Hybrid Central Tower technology have not been found.

Therefore, the purpose of this paper is to evaluate the economic potential of the CSP_{th} Hybrid Central Tower technology through the levelized cost of heat, so a wide range of industries might have a clear notion of the competitiveness of this renewable technology against the conventional sources of energy. The paper includes a sensitivity assessment that considers changes in the solar resource, the investment cost (capital expenditure-CAPEX), the O&M expenses, the discount rate, and the solar multiple. The study also includes an estimation of the avoided greenhouse gas emissions and the marginal abatement costs. Section 1 gives a short review of process heating systems and mentions the feasibility of solar thermal technologies for process heating, Section 2 describes the methodology of this work, Section 3 presents some characteristics of the CSP_{th} Hybrid Central Tower systems designed for a reference location, Section 4 presents results and discussions, and Section 5 presents the conclusions of this work.

Feasibility of Solar Thermal Technologies for Industrial Process Heating

Process heating systems can be broken into three basic categories: fuel-based process heating, electric-based process heating, and steam-based process heating [28]. The process characteristics define the selection of the heating system; the process can be either a discrete or a continuous process and require either a direct or an indirect heating method. Industrial processes often take energy from a heat transfer medium (indirect method). Heat transfer mediums should have a low vapor pressure, high heat capacity, low viscosity, high thermal stability, and low corrosiveness [29]; common mediums are steam, pressurized water, thermal oil, and air.

Steam-based systems supply around 30% of the industrial energy consumption worldwide [30]. Steam is an efficient energy carrier; it can be used to control temperature and pressure of chemical processes, remove contaminants, and other miscellaneous applications [28]. Hot air is commonly used at temperatures around 250 °C for drying processes, which are highly relevant in the industry. Hot air is produced either by electrical heating or using a heat transfer medium [31]. Table 1 lists common applications of process heat and the temperature range of these processes.

Table 1. Temperature range of common industrial processes [32].

Industry	Process	Temperature (°C)
Cross-cutting	Water preheating	60–90
	Washing	60–90
Food and Beverages	Pasteurization	60–80
	Concentration	60–80
	Cooking	60–100
	Sterilization	60–120
	Blanching	75–90
	Drying	120–180
Textiles	Bleaching/dyeing	60–90
	Pressing	80–100
	Drying	100–130
	Fixing	160–180
Paper and Wood Products	Cooking/drying	60–80
	Pulp preparation	120–170
	Bleaching	130–150
Plastics	Preparation	120–140
	Blending	120–140
	Extension	140–160
	Distillation	140–290
	Drying	180–200
	Separation	200–220
Petroleum Refining	Distillation	370–425
Chemicals	Drying/distillation	170–230
	Steam reforming	500–900
Nonmetallic Minerals	Preheating	200–750
	Calcination (dry)	750–1000
	Sintering	1200–1450
Primary Metals	Precipitation	200–300
	Annealing	300–500
	Reduction (ore)	1000–1100

Renewable technologies allow energy consumers to use clean energy sources, reducing their fossil fuel dependency. Among renewable energies, solar energy is the most abundant energy source in the planet; it is related to energy self-sufficiency, energy access in isolated areas, and employment creation [33]. Solar thermal energy is a suitable option for industrial process heating; whereas the conversion efficiency from solar energy to electricity is between 15 and 20%, the conversion efficiency from solar energy to thermal energy is up to 70% [29].

Table 2 summarizes the temperature range of non-concentrating and concentrating solar thermal technologies. The maximum operating temperature of the current commercial systems is about 600 °C [34], which corresponds to the Central Tower technology; however, temperatures of about 800 °C have been achieved using air as the heat transfer medium [35–37].

Table 2. General features of the solar thermal technologies [38].

Parameter	Type of Technology						
	Flat Plate Collectors	**Evacuated Tube Collectors**	**Compound Parabolic Collectors**	**Linear Fresnel Systems**	**Parabolic trough Systems**	**Parabolic Dish Reflector**	**Central Tower Systems and Solar Furnaces**
Absorber Type	Flat	Flat	Linear	Linear	Linear	Point	Point
Concentration ratio	1	1	1–5	10–40	15–45	100–1000	100–1500
Temperature range (°C)	30–80	50–200	60–240	60–250	60–300	100–500	150–2000

Industrial processes require a stable energy source because the stability defines both the process efficiency and the quality of products. In this sense, CSP_{th} systems have two advantages: CSP_{th} systems can use thermal energy storage (TES) systems and operate in combination with fuel-based systems. TES systems are low-cost and highly efficient methods to store energy and mitigate short fluctuations. Operating temperature of commercial TES systems can reach about 585 °C for CSP_{th} Central Tower systems [39].

2. Methodology

The methodology consisted of five major steps: (1) defining the CSP_{th} Hybrid-CT system, (2) generating the layout of the CSP_{th} Central Tower (using SolarPILOT), (3) evaluating the layout's performance, (4) evaluating the steady-state energy balance of the CSP_{th} Hybrid-CT system, and (5) estimating the *LCOH* of the CSP_{th} Hybrid-CT system. Three geographic sites were chosen to carry out the analysis. These locations correspond to Hermosillo, Sonora (annual DNI 2680 kWh/m^2); Altamira, Tamaulipas (annual DNI 1851 kWh/m^2); and the Region of Antofagasta, Chile (annual DNI 3576 kWh/m^2).

2.1. Definition of the CSP_{th} Hybrid-CT System and Suppositions for the Analysis

Figure 1 presents a general scheme for the CSP_{th} Hybrid-CT system. The figure shows the plant configuration and the major components of the system: heliostat field, tower, receiver, TES system, steam-generation system (SGS), and fuel-based boiler. Auxiliary components of the system are not considered in the analysis; therefore, the *LCOH* results are not weighted by the energy parasitics, which usually accounts for about 10% of the electricity output in power generating systems [40].

The heliostat field reflects the solar irradiation to the receiver device; as the irradiation is absorbed, the receiver's temperature increases, this allows the receiver to transfer thermal energy to a fluid. The common heat transfer fluid is molten salt [41]. After being heated, the molten salt is sent to the hot-tank for further dispatching to a steam generation system. The fuel-based boiler operates if there is not enough solar energy to fulfill the heat demand.

Data from McMillan and Mark [25] suggest that alternative heat generators, such as Concentrating Solar Technologies, that can provide thermal power outputs between 10 MW_{th} and 200 MW_{th} are potentially applicable to several industries. In this sense, a design thermal power output of 50 MW_{th} was used for the analysis.

The analysis of the CSP_{th} Hybrid-CT system was performed considering the following assumptions:

- Just the major components of the CSP_{th} Hybrid system were considered.
- The system's performance was evaluated throughout the year, using time steps of 1 h.
- The system was considered to operate in steady-state.
- The annual energy production was assumed constant for the system's lifespan.
- Pressure drops were neglected.
- Electrical parasitics were not considered.
- The fuel-based boiler was considered to operate with natural gas.
- The fuel-based boiler's efficiency was considered to be 85%, which corresponds to high level efficiency [30].
- The system's lifespan was considered to be 30 years.

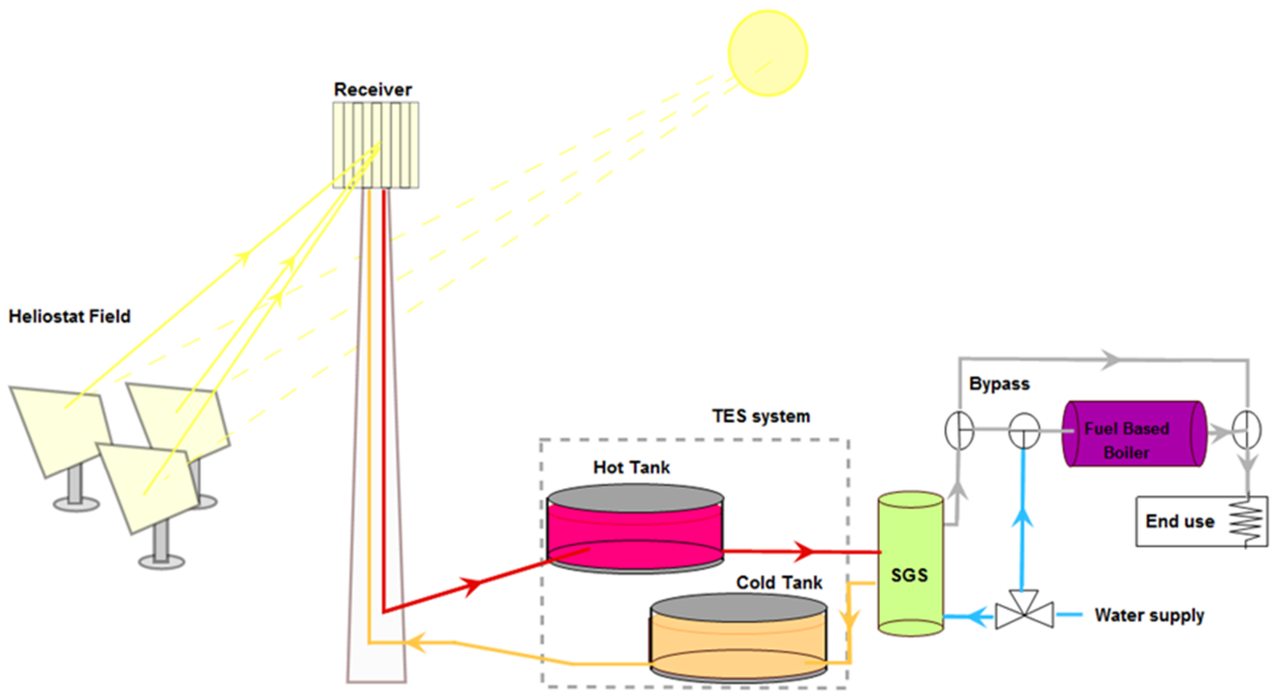

Figure 1. Diagram of a CSP_{th} Hybrid-CT system.

2.2. Layout of the CSPth Central Tower

The CSP_{th} Central Tower was designed using SolarPILOT. This software provides layout, characterization, optimization capabilities, and parametric simulation [42].

Several layouts were generated to evaluate the effect of the solar multiple. The solar multiple (S.M.) is the ratio between the energy delivered by the system when it operates at design conditions and the nominal energy demand.

The general procedure to generate every layout was as follow:

1. Selection of a thermal power.
2. Selection of the design point.
3. Generation of the layout.
4. Optimization of the layout based on the system's performance.

Two parameters define de design point (item 2): the sun position for the layout generation and the design direct normal irradiation (DNI). The layouts were generated for the noon of the spring equinox. The design DNI is a highly relevant parameter: a low design DNI value generates an oversized solar field, increasing the capital expenditure; on the contrary, a high design DNI value generates an undersized solar field, which results in poor performance most of the year. The design DNI value was selected after evaluating the performance of six layouts that were generated with different DNI values.

2.3. Energy Balance of the CSP_{th} Hybrid-CT System

The energy that the receiver transfers to the heat transfer fluid was calculated using the following procedure (steps 1–4):

1. The optical efficiency of the solar field was evaluated at 146 sun positions.
2. For every hour of the year between the sunrise and the sunset, the efficiency value was taken from the nearest sun's position that was evaluated in step 1.
3. For every hour before sunrise and after sunset, the solar field's efficiency was fixed at zero.
4. The energy that the heat transfer fluid absorbs was calculated with Equation (1).

$$E_{Solar_i} = \eta_{SF_i} DNI_i A_{SF} - Q_{R-loss} \tag{1}$$

i: Hour of the year [index].
A_{SF}: Solar field's area [m^2].
DNI_i: Direct Normal Irradiation [W/m^2].
η_{SFi}: Solar field's efficiency [%].
$Q_{R\text{-}Loss}$: Receiver's heat loss [W/m^2].

For this work, "$Q_{R\text{-}Loss}$" was assumed constant at a typical value of 30 kW/m^2 [43]; as a consequence of keeping a constant "$Q_{R\text{-}Loss}$", the product "$\eta_{SFi} DNI_i A_{SF}$" can be lower than "$Q_{R\text{-}Loss}$" for low DNI values or low solar field´s efficiencies. In these cases, "E_{Solari}" was changed by zero.

The energy balance of the TES system was calculated with Equation (2).

$$\frac{dTES_i}{dt} = h_{in} \frac{dm_{in_i}}{dt} - h_{out} \frac{dm_{out_i}}{dt} - \frac{dQ_{loss_i}}{dt} \tag{2}$$

$dTES_i/dt$: Energy change in the TES system at time i [J/h]
$h_{in}(dm_{ini}/dt)$: Energy entering the system at time i [J/h]
$h_{out}(dm_{outi}/dt)$: Energy entering the system at time i [J/h]
$dQloss_i/dt$: Energy loss at the TES system [J/h]

Kolb [43] estimates a thermal energy loss of 1 MW_{th} for a TES system of 5000 MWh; this represents an hourly loss of 0.02%. For this work, the energy loss at time "i" was assumed to be 1% of the stored energy at time "$i - 1$".

$$\frac{dQ_{loss_i}}{dt} = 0.01\ TES_{i-1} \tag{3}$$

Equations (4)–(7) were used to calculate the charging and discharging process of the TES system.

$$h_{in} \frac{dm_{in\_i}}{dt} = \begin{cases} 0 & ;\ if\ \eta_P\ \eta_{SG} E_{Solar_i} \le E_D \\ E_{Solar-TES_i} & ;\ if\ \eta_P\ \eta_{SG} E_{Solar_i} > E_D \end{cases} \tag{4}$$

$$E_{Solar-TES_i} == \begin{cases} E_{Solar_i} - (E_D/\ \eta_P\ \eta_{SG}) & ;\ if\ TES_{i-1} + E_{Solar_i} - (E_D/\ \eta_P\ \eta_{SG}) \le SE_{U-lim} \\ SE_{U-lim} - TES_{i-1} & ;\ if\ TES_{i-1} + E_{Solar_i} - (E_D/\ \eta_P\ \eta_{SG}) > SE_{U-lim} \end{cases} \tag{5}$$

$$h_{out} \frac{dm_{out_i}}{dt} = \begin{cases} 0 & ;\ if\ \eta_P\ \eta_{SG} E_{Solar_i} \ge E_D\ or\ TES_{i-1} = SE_{L-lim} \\ E_{TES-HTF_i} & ;\ if\ \eta_P\ \eta_{SG} E_{Solar_i} < E_D\ and\ TES_{i-1} > SE_{L-lim} \end{cases} \tag{6}$$

$$E_{TES-HTF_i} == \begin{cases} (E_D/\eta_P\ \eta_{SG}) - E_{Solar_i} & ;\ if\ TES_{i-1} + E_{Solar_i} - (E_D/\eta_P\ \eta_{SG}) \ge SE_{L-lim} \\ TES_{i-1} - SE_{L-lim} & ;\ if\ TES_{i-1} + E_{Solar_i} - (E_D/\eta_P\ \eta_{SG}) < SE_{L-lim} \end{cases} \tag{7}$$

E_D: Energy demand per hour (50 MWh)
η_P: Thermal efficiency of pipelines [%]. This value was assumed to be 98%.
η_{SG}: Efficiency of the steam generation system [%]. This value was assumed to be 95%.
$SE_{U\text{-}lim}$: Upper charging limit of the TES system [J]
$SE_{L\text{-}lim}$: Lower discharging limit of the TES system [J]

The fuel consumption was calculated using Equations (8) and (9).

$$FC_i == \begin{cases} \left(E_D - \eta_P\ \eta_{SG} E_{Solar_i}\right)/\eta_P \eta_B & ;\ if\ \eta_P\ \eta_{SG} E_{Solar_i} \le E_D\ and\ TES_{i-1} = SE_{L-lim} \\ E_{F-HTF_i}/\eta_P \eta_B & ;\ if\ \eta_P\ \eta_{SG} E_{Solar_i} \le E_D\ and\ TES_{i-1} > SE_{L-lim} \end{cases} \tag{8}$$

$$E_{F-HTF_i} == \begin{cases} 0 & ;if\ \eta_P\ \eta_{SG}\left(E_{Solar_i} + E_{TES-HTF_i}\right) = E_D \\ E_D - \eta_P\ \eta_{SG}\left(E_{Solar_i} + E_{TES-HTF_i}\right) & ;if\ \eta_P\ \eta_{SG}\left(E_{Solar_i} + E_{TES-HTF_i}\right) < E_D \end{cases} \tag{9}$$

η_b: Efficiency of the fuel-based boiler [%]

2.4. Cost of the CSP_{th} Hybrid-CT System

The cost of the CSP_{th} Hybrid-CT system was separated into direct and indirect costs (Equation (10)). The direct costs consist of the capital expenditure related to the main components of the CSP_{th} Hybrid-CT system (Equation (11)); the indirect costs were calculated as a percentage of the direct costs. Indirect costs include several owner's costs: land cost, planning and contracting costs, engineering and construction management, and contingency costs [44].

$$SC = DC + IC \quad (10)$$

$$DC = (HF_C + T_C + R_C + TES_C + SGS_C + B_C) \quad (11)$$

HF_C: Heliostats field cost (USD)
T_C: Tower cost (USD)
R_C: Receiver cost (USD)
TES_C: TES system cost (USD)
SGS_C: Steam generation system cost (USD)
B_C: Fuel-based boiler cost (USD)

Table 3 summarizes the reference data for the cost of the system´s components. The heliostat field cost was calculated by multiplying the heliostat field area by a solar field price. Although a solar field price of 150 USD/m^2 is used in the most recent reference of Table 3, for this work a conservative value of 200 USD/m^2 was assumed for the analysis. The TES system cost was calculated by multiplying the TES capacity by 30 USD/kW_{th}. The tower cost was calculated with an exponential function, Equation (12) [45]. The receiver cost, the steam generation system cost, and fuel-based boiler cost were calculated using a capacity function, Equation (13) [45].

$$T\ cost = C_k e^{(s)H} \quad (12)$$

$$C_x = C_R (S_x/S_R)^s \quad (13)$$

C_X: Estimated cost of equipment of size "S_x" (USD)
C_R: Reference cost of equipment of size "S_R" (USD)
H: tower's height (m)
S: scaling exponent ().

The scaling exponents were 0.0113 for the tower, 0.7 for the receiver, and 0.8 for both the steam generation system and the fuel-based boiler [45]. The reference costs in Table 3 were actualized for Equation (13). The actualizations were carried out using the Chemical Engineering Plant Cost Index 2019 (CEPCI 2019), Equation (14).

$$C_R = C(I_L/I_O) \quad (14)$$

C: reference cost at year of reference (USD)
I_L: Index of the CEPCI 2019
I_O: Index of the CEPCI at the reference year.

Table 3. Reference costs for the CSP_{th} Hybrid-CT system.

Equipment	Reference Cost (year)	References	Costs Used for This Work
Solar Field	130–217 \$USD/m^2	[27,46–54]	200 \$USD/m^2
Tower	28,500,000 USD; Size: 203 m (2010)	[45]	3,170,000 $e^{0.0113H}$
Receiver	97,020,000 USD; Size: 1571 m^2 (2010)	[45]	107,020,000 USD; Size: 1571 m^2
Storage	14–33 \$USD/kWh_{th}	[47–49,51–53]	30 USD/kWh_{th}

Table 3. *Cont.*

Equipment	Reference Cost (year)	References	Costs Used for This Work
Steam Generation	29,000,000 USD; Size: 260 MW_{th} (2011)	[48]	9,408,000 USD; Size: 50 MW_{th}
Fuel-Based Boiler	4,200,000 USD; Size: 26.6 MW_{th} (2015)	[55]	8,018,830 USD; Size: 50 MW_{th}
Indirect Cost	15–17 (% of D.C.)	[47,51,53]	15%

2.5. LCOH Calculation

The levelized cost of heat (*LCOH*) is analogous to the levelized cost of energy (LCOE), which is the common economic measure for electric power generation systems [56,57].

The *LCOH* can be defined as the average cost in net present value (NPV) of a unit of heat that is produced by a system. The NPV of the costs incurred during the system's lifespan must equal the NPV of all the annual energy production multiplied by the *LCOH* in the same period (Equation (15)). The *LCOH* was calculated using Equation (16).

$$\sum_{n=0}^{N} \frac{Costs_n}{(1+r)^n} = \sum_{n=0}^{N} \frac{AEP * LCOH}{(1+r)^n} \tag{15}$$

$$LCOH = \left(CAPEX + \sum_{n=1}^{N} \frac{Costs_n}{(1+r)^n} \right) \Big/ \sum_{n=1}^{N} \frac{AEP}{(1+r)^n} \tag{16}$$

LCOH: Levelized cost of heat (Cents USD/kWh_{th})
AEP: Annual energy production of the CSP_{th} Hybrid-CT system (MWh_{th})
CAPEX: Capital expenditure (USD)
$Costs_n$: Annual costs incurred at year "n" (USD)
r: Discount rate (%)
N: System´s lifespan ()

In Equation (16), the capital expenditure is not discounted since it occurs at time 0. The annual costs that are discounted comprise four concepts: operation and maintenance expenses "*O&M*", insurance "*I*", annual fuel expenses "*FE*", and a carbon price for the CO_2 emissions (see Section 2.6). Insurance was considered for this analysis because it is an efficient mechanism to avoid the high economic risks associated with non-mature technologies. Table 4 shows the values used for the O&M expenses, insurance, and the lifespan. A discount rate of 8% was used to calculate the *LCOH*. The *LCOH* was calculated at constant value (2019 dollars).

Table 4. O&M costs, insurance, and lifespan for the *LCOH* calculation.

	Reference Value	References	Value Used in This Work
O&M (% of CAPEX)	1–2.5%	[27,47,58–62]	2%
O&M Fuel-Based Boiler	0.95 USD/MMBTU of Fossil Fuel input	[55]	0.95 USD/MMBTU of Fossil Fuel input
Insurance (% of CAPEX)	0.5–1	[27,46,47,51,53,54,56,58–60,62]	0.5%
Lifespan	25–30 years	[27,46,47,51,53,54,56,58–62]	30 years

The annual fuel expenses "FE_n" were calculated considering the annual fuel consumption and the fuel price of natural gas (Equation (17)).

$$FE_n = FP_n \sum_{i=1}^{8760} FC_i \tag{17}$$

FP_n: Fuel price of natural gas at year "n" in 2019 dollars (USD)

FC_i: Fuel consumption at time "i" (J)

The price of natural gas is considerably different around the world [63] in this sense, the *LCOH* was calculated for several fuel price scenarios (FPS) (see Table 5). To include the change in real terms of the natural gas price over time, an arithmetic gradient was applied to the initial fuel price (price in 2019). This gradient was calculated based on the price projections of the U.S. Energy Information Administration (EIA) for the natural gas spot price at Henry Hub. EIA suggests for the reference case that the natural gas spot price will be approximately 3.8 USD/MMBTU by 2050 (in 2019 dollars) [64]. This implies an increase in real terms of approx. USD 0.04 per year considering that the natural gas price was 2.56 USD/MMBTU in 2019 [65].

Table 5. Fuel price scenarios (prices in 2019 dollars).

Fuel Price Scenario	USD/MMBTU (2019 Dollars)	
	Year 2019	Year 2050
FPS 3	3	4.2
FPS 5	5	6.2
FPS 7	7	8.2
FPS 9	9	10.2
FPS 11	11	12.2

2.6. Pricing CO_2 Emissions

Carbon pricing creates a financial incentive that drives technological innovation and investment in clean energy. Explicit carbon prices are introduced through taxes on fossil fuels or by putting a price on GHG emissions; additionally, emissions are regulated using carbon market systems. There are two types of carbon markets: Emission Trading Systems (ETS) and Baseline-and-Credit mechanisms [66]. In carbon markets, the price of allowances or credits for compliances vary regarding local regulations (see Table 6).

Table 6. Examples of carbon markets in operation. Source: [67,68].

Emission Trading Systems:	**Coverage**	**Allowance Price**
China National ETS	4000 $MtCO_2$	Free allocation
European Union ETS	1610 $MtCO_2e$	Free Allocation & Auction; 28.28 USD/tCO_2e
California Cap-And-Trade Program	320 $MtCO_2e$	Free Allocation & Auction; 17.04 USD/tCO_2e
Credit Mechanisms:	Credits Issued	Credit Price
Clean Development Mechanism	74 $MtCO_2e$	2.02→USD/tCO_2e
Verified Carbon Standard	140.37 $MtCO_2e$	1.62→USD/tCO_2e
California Compliance Offset Program	46 $MtCO_2e$	13.71 USD/tCO_2e

Today, 21.5% of the global GHG emissions are covered by carbon pricing instruments [68]. However, nowadays, most carbon prices remain far below the range needed to help meet the limit of 1.5 °C [69]. The High-Level Commission on Carbon Prices suggests that a carbon price consistent with the Paris Agreement's goal should be at least 40–80 USD/tCO_2e by 2020 and 50–100 USD/tCO_2e by 2030 [70].

One instrument that is gaining momentum is the voluntary carbon pricing. Currently, nearly half of the world's 500 biggest companies use or plan to use this instrument [71]. Companies use this instrument to address the risk of an increase in the price of GHG emissions. The common types of internal carbon prices are the internal fee, which produces actual financial flows, and the shadow price, which is a hypothetical cost to evaluate investments decisions. In 2020, the median internal carbon price disclosed by companies was 25 USD/tCO_2e [71].

For this work, the *LCOH* (Equation (16)) was calculated considering a shadow price in line with the recommendations of the High-Level Commission on Carbon Prices. The *LCOH* was calculated with a price of 40 USD/tCO_2e for the first 10-years period, 50 USD/tCO_2e for the second 10-years period, and 60 USD/tCO_2e for the last 10-years period.

2.7. Marginal Abatement Cost

Compared to fuel-based systems, CSP_{th} Hybrid-CT systems provide energy with low rates of CO_2 emissions. The CO_2-avoided emissions were calculated using Equation (18).

$$AE_{CO2} = R_{E-CO2}\left((AEP/\eta_P\eta_B) - \sum_{i=1}^{8760} FC_i \right) \quad (18)$$

$R_{E\text{-}CO2}$: Emission factor [Kg of CO_2/MWh]
AEP: Annual energy production of the CSP_{th} Hybrid-CT system [MWh_{th}]
For natural gas, $R_{E-CO2} = 0.20196$ ton of CO_2/MWh [72].

The marginal abatement costs are defined as the estimated cost of avoiding a ton of CO_2 emissions. This value is often used as a reference to establish the carbon price needed to trigger abatement measures. The marginal abatement cost was calculated with Equation (19). To obtain the real value of the marginal abatement costs, the *LCOH* of the CSP_{th} Hybrid-CT system and *LCOH* of the Fuel-Based system were calculated without pricing the CO_2 emissions.

$$MAC = \frac{AEP(LCOH - LCOH_{F-B\ S})}{AE_{CO2}} \quad (19)$$

LCOH: LCOH of the CSP_{th} Hybrid-CT system
$LCOH_{F\text{-}BS}$: *LCOH* of a Fuel-Based system

3. Technical Characteristics of the CSP_{th} Hybrid-CT Systems Designed for the Reference Location

The reference location corresponds to Hermosillo, Sonora, Mexico (latitude 29° and longitude −110°). The solar resource data were taken from the NREL National Solar Radiation Database [73]. The Typical Meteorological Year data (annual DNI = 2680 kWh/m^2) was used to evaluate the annual energy production.

The design DNI value was chosen after comparing the technical and economic results of six systems designed with different DNI values. Figure 2 shows how the design DNI value affect both the *LCOH* of the CSP_{th} Central Tower and the solar energy contribution. In general, increasing the design DNI value leads to a reduction in the solar energy contribution. The minimum *LCOH* (6.37 Cents/kWh_{th}) corresponds to a design DNI of 800 W/m^2; this *LCOH* was calculated considering just the solar energy contribution. Figure 2 shows the excess of solar energy and the percentage of the annual energy production that is produced when the thermal power of the CSP_{th} Central Tower is below 50 MW_{th}. The excess of solar energy occurs when the CSP_{th} Central Tower produces more energy than the energy demand. The first parameter shows that the solar field is oversized for design DNI values below 800 W/m^2; on the contrary, the second parameter shows that the solar field is undersized for design DNI values above 800 W/m^2.

However, the *LCOH* of the CSP_{th} Hybrid-CT system changes if considering both the solar energy contribution and the energy that is produced with fossil fuel. Figure 3 show the effect of the design DNI value on both the solar fraction and the *LCOH*. An increase in the solar fraction leads to an increase in the *LCOH*; to clearly show this effect, the *LCOH* values were calculated without pricing the CO_2 emissions. Figure 3 shows the capital expenditure for the system.

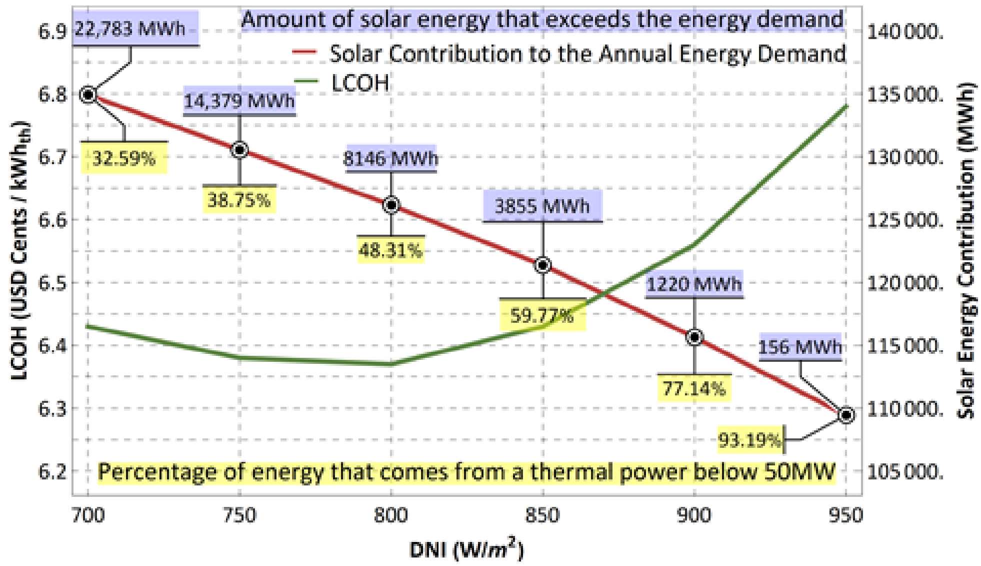

Figure 2. Influence of the design DNI value on the annual energy production and the *LCOH* of the CSP_{th} Central Tower.

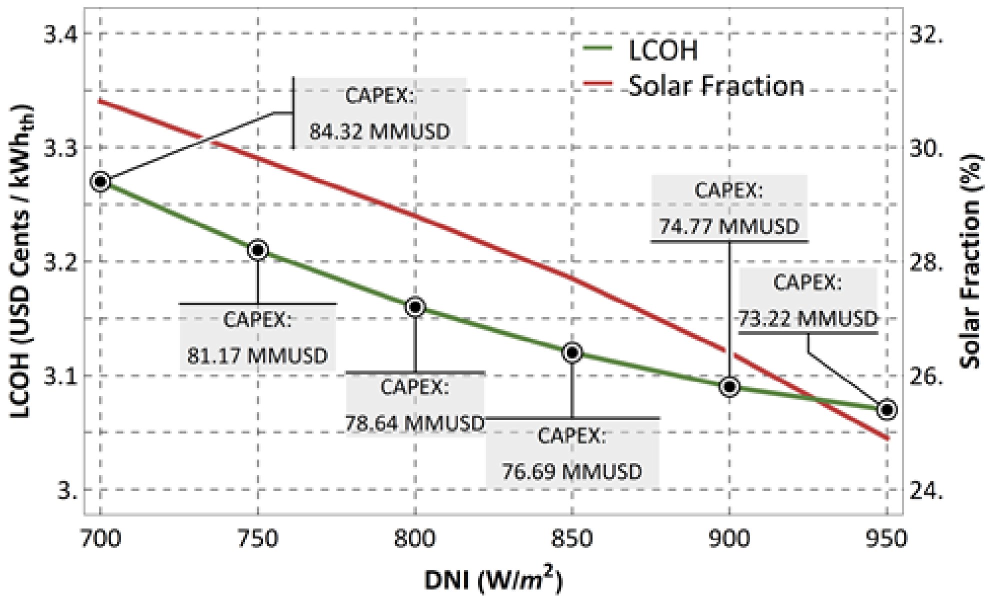

Figure 3. Influence of the design DNI value on the solar fraction and the *LCOH* of the CSP_{th} Hybrid-CT system.

Considering the results of Figures 2 and 3, the value of 800 W/m^2 was selected to be the design DNI. Figure 4 shows the layout of the CSP_{th} Central Tower; the figure shows the solar field's arrangement and the heliostats' efficiencies at the design point. The solar field achieves an optical efficiency of 57.41%, including the receiver's efficiency. A typical constrain for tubular receivers is the incident flux; this parameter is usually kept below 1200 kW/m^2 in order to avoid fractures and to conserve the shape and strength of the receiver. The average incident flux and the peak incident flux are 467 kW/m^2 and 1130 kW/m^2, respectively; these values were obtained using SolTrace.

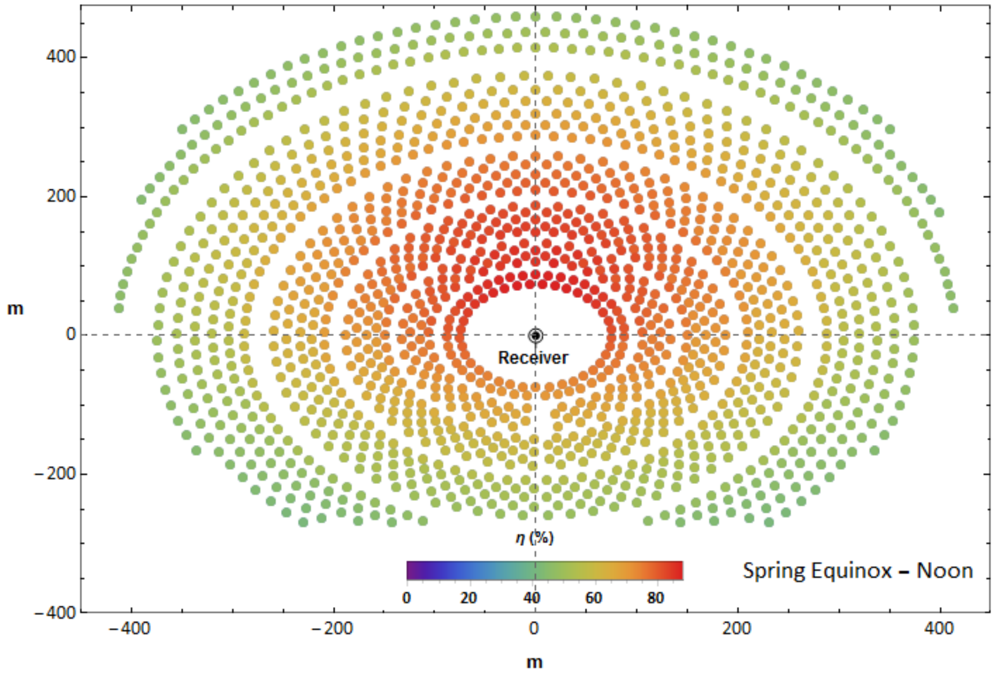

Figure 4. Solar field´s arrangement and heliostats' efficiencies at the design point.

Figure 5 shows the optical efficiency of the system at 146 sun positions. Because the solar resource and the optical efficiencies vary throughout the year, the CSP_{th} Central Tower operates at off-design most of the time; therefore, the heat transfer fluid absorbs different rates of thermal power per hour. Figure 6 shows the thermal power absorbed by the heat transfer fluid. Annually, the system delivers around 128,747 MWh of solar thermal energy.

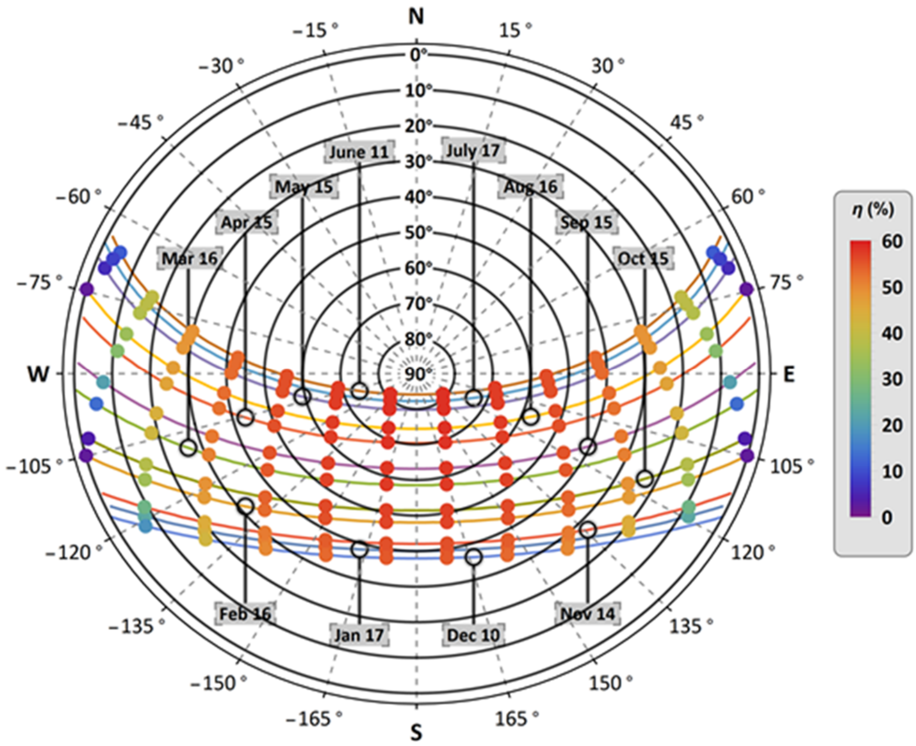

Figure 5. Optical efficiency of the CSP_{th} Central Tower at 146 sun positions.

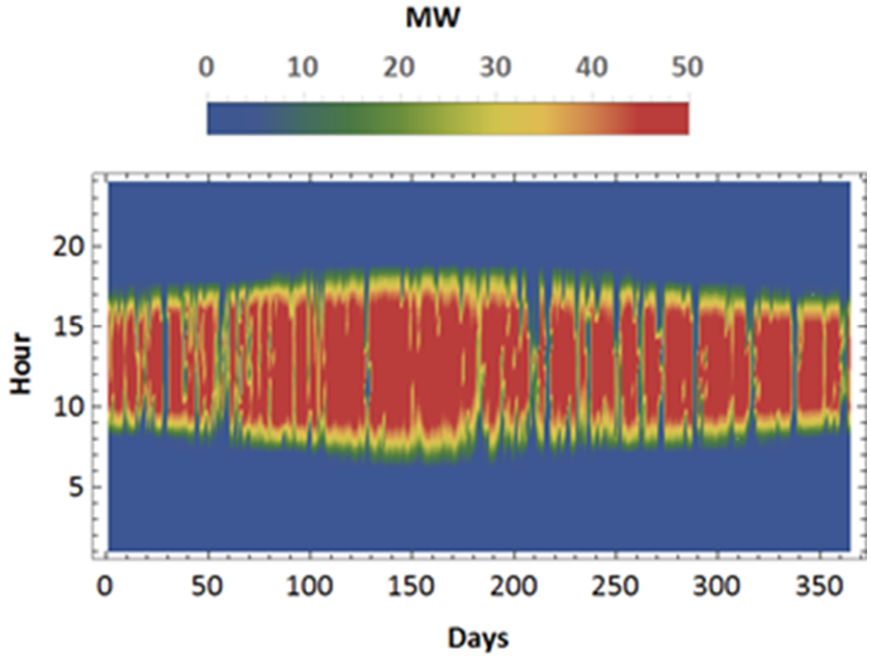

Figure 6. Thermal power absorbed by the heat transfer fluid throughout the year.

To increase the solar energy contribution, the CSP_{th} Central Tower was designed with solar multiples of 1.5, 2, and 2.5; a thermal energy storage system has been included in the analysis of these systems. The amount of stored energy depends strongly on the season. Figure 7 shows how the TES capacity determines the amount of stored energy during the summer and winter solstices. At the summer solstice, the CSP_{th} Central Tower produces an energy surplus equivalent to 11 h of energy demand; however, at the winter solstice the energy surplus is equivalent to 6 h of energy demand.

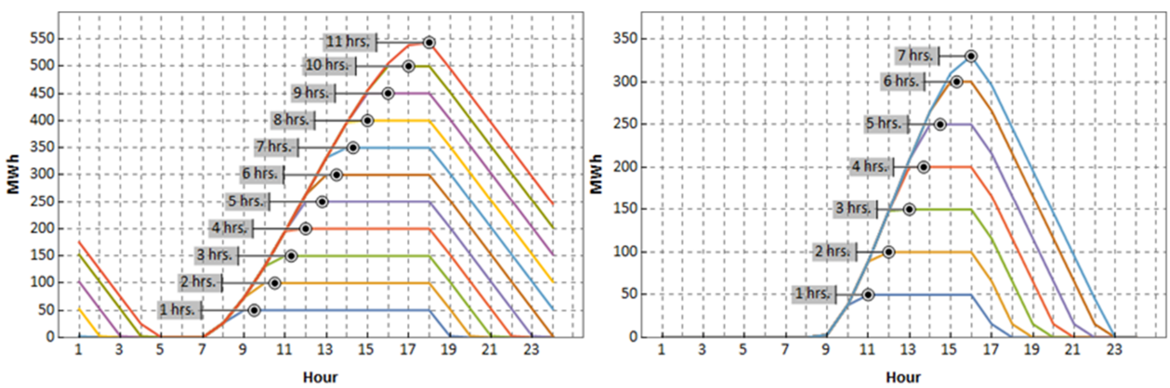

Figure 7. Variation of stored energy at the summer (**left**) and winter (**right**) solstices for different TES capacities. Solar multiple = 2.

The TES capacity was chosen after calculating the *LCOH* of the CSP_{th} Central Tower systems for different TES capacities; this *LCOH* was calculated considering just the solar energy contribution. Figure 8 shows that the minimum *LCOH* for the systems designed with solar multiples of 1.5, 2, and 2.5 was achieved with TES capacities of 5, 9, and 13 h, respectively.

Table 7 presents some characteristics of the CSP_{th} Hybrid-CT systems that are further analyzed in Section 5. The increase in capital expenditure between these systems results in significant increases of the solar fraction.

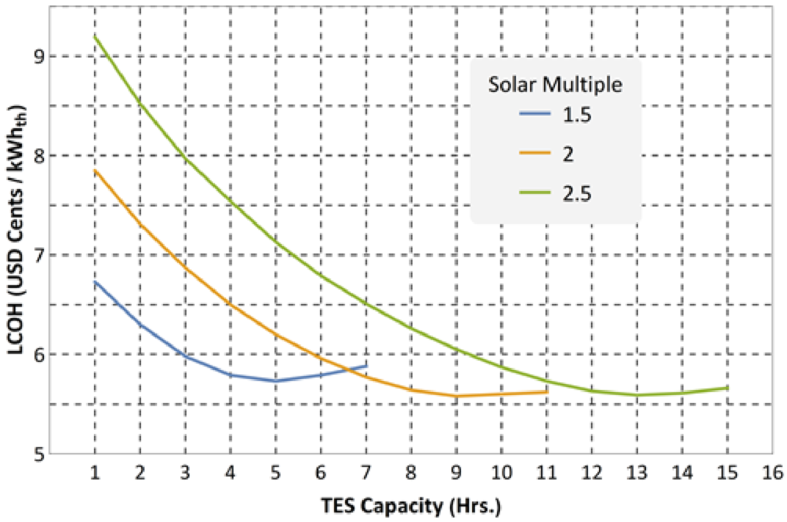

Figure 8. Influence of the TES capacity on the *LCOH* of the CSP_{th} Central Tower.

Table 7. Technical characteristics of the CSP_{th} Hybrid-CT systems.

Heliostat Field				
Solar Multiple	1	1.5	2	2.5
Num. Heliostats	1480	2252	2977	3612
Heliostat field area (m^2)	116,284	176,940	233,903	283,795
Design power (MW_{th})	50	75	100	125
Receiver				
Area (m^2)	142.9	200.27	251.32	345.57
Optical Efficiency (%)	90	90	90	90
Tower optical height	90	105	125	140
Storage				
Capacity (hours)	-	5	9	13
Capacity Power (MWh)	-	250	450	650
Steam Generation System				
Capacity (MW_{th})	50	50	50	50
Fuel-Based System				
Capacity (MW_{th})	50	50	50	50
Annual Energy Production (MWh)	438,000	438,000	438,000	438,000
Solar contribution (MWh)	128,747	204,825	268,955	329,639
Backup fuel contribution (MWh)	309,253	233,175	169,045	108,361
Solar Fraction (%)	29.39	47.76	61.4	75.26
Capital Expenditure USD				
Heliostat Field	23,256,800	35,388,000	46,780,600	56,759,000
Receiver	19,983,600	25,304,700	29,663,900	37,071,500
Tower	8,764,690	10,383,600	13,016,700	15,421,000
Storage	-	7,500,000	13,500,000	19,500,000
Steam Generation System	9,408,000	9,408,000	9,408,000	9,408,000
Fuel-Based System	8,018,830	8,018,830	8,018,830	8,018,830

Table 7. *Cont.*

Sub-Total	69,431,920	96,003,130	120,388,030	146,178,330
Indirect Costs (15%)	10,414,788	14,400,469	18,058,204	21,926,749
System Cost	79,846,708	110,403,599	138,446,235	168,105,080

4. Results and Discussions

This section presents the results that were obtained using the methodology of Section 3. First, the section shows the *LCOH* of the CSP_{th} Hybrid-CT systems of Table 7 (reference location) and the *LCOH* of a fuel-based system. The section includes a sensitivity analysis. Then, the section presents the *LCOH* of the CSP_{th} Hybrid-CT systems considering a 20% reduction in the CAPEX of the CSP_{th} Central Tower and using a discount rate of 5%. Finally, the section presents the avoided CO_2 emissions and the marginal abatement costs for this technology.

Figure 9 shows the *LCOH* of the CSP_{th} Hybrid-CT systems and the *LCOH* of a fuel-based system. For the fuel price scenario of 3 USD/MMBTU, the *LCOH* of the CSP_{th} Hybrid-CT system (S.M. 1) is 4.04 USD Cents/kWh_{th}. The *LCOH* increases for higher prices of fossil fuel; for example, the *LCOH* is 4.63 USD Cents/kWh_{th} for the case of 5 USD/MMBTU. Moreover, the *LCOH* increases for systems designed with solar multiples bigger than 1. For example, using the fuel price scenario of 3 USD/MMBTU, the *LCOH* of the system designed with a solar multiple of 2.5 is 5.05 USD Cents/kWh_{th}. However, there is a point where increasing the solar fraction results positive: at 9 USD/MMBTU, the *LCOH* of the CSP_{th} Hybrid-CT system (S.M. 2.5) is lower than the *LCOH* of the CSP_{th} Hybrid-CT systems designed with lower solar multiples. Two reasons explain this: First, the O&M costs of the fuel-based boiler are proportional to the fossil fuel consumption; second, CSP_{th} Hybrid-CT systems with higher rates of fossil fuel consumption are more sensitive to fuel prices. The second fact is evident by looking at the slope of each system in Figure 9. The breakeven point (fuel price scenario) at which the *LCOH* of the CSP_{th} Hybrid-CT system equals the *LCOH* of the fuel-based system changes regarding the solar multiple; however, this point is about 9.5 USD/MMBTU for the CSP_{th} Hybrid-CT system designed with a solar multiple 2.5.

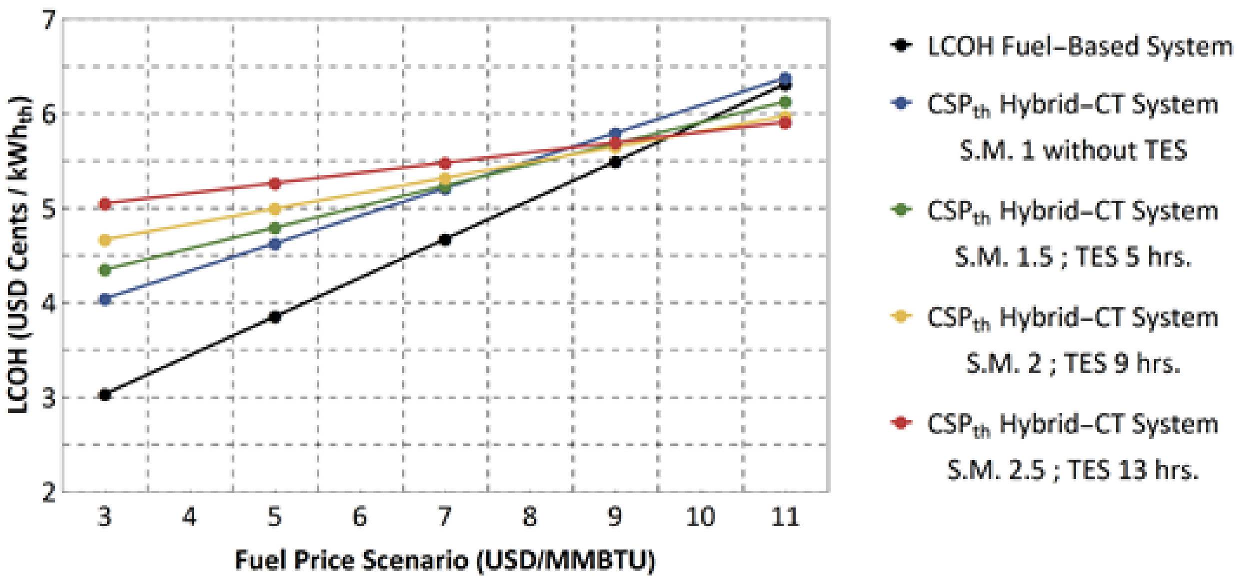

Figure 9. *LCOH* of the CSP_{th} Hybrid-CT systems of Table 7.

The *LCOH* depends on four major factors: solar resource, capital expenditure, discount rate, and O&M costs. Figure 10 shows a sensitivity analysis for the *LCOH* of the CSP_{th} Hybrid-CT systems of Table 7. The reference case corresponds to the *LCOH* for the fuel price scenario of 7 USD/MMBTU.

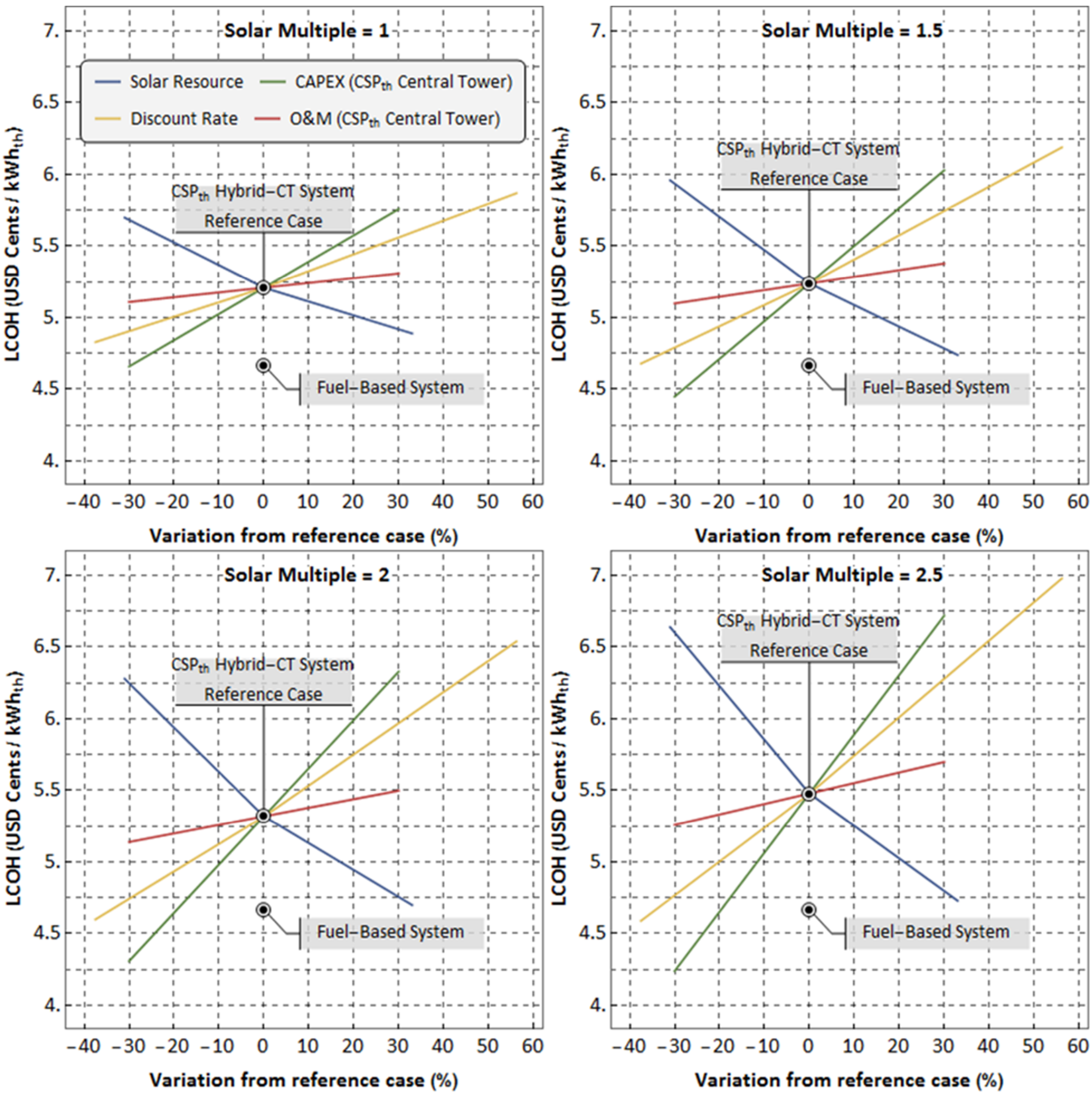

Figure 10. Sensitivity analysis for the *LCOH* of the CSP_{th} Hybrid-CT systems.

To estimate the effect of the solar resource, the CSP_{th} Hybrid-CT systems were designed for two different locations; the calculations described in Section 4 were carried out for these locations. One location corresponds to the state of Tamaulipas, Mexico, which presents an annual DNI of 1851 kWh/m^2 (latitude 22.4° and longitude −97.9°); the DNI data were taken from the NREL National Solar Radiation Database [73]. The other location corresponds to the region of Antofagasta, Chile, which presents an annual DNI of 3576 kWh/m^2 (latitude −23.7 and longitude −70.1); the DNI data were taken from the Solar Exploratory of the Ministry of Energy of Chile [74].

To evaluate the effect of the capital expenditure, the *LCOH* was calculated considering a change of ±30% in this parameter; this change was applied just to the capital expenditure that corresponds to the CSP_{th} Central Tower. Two scenarios were used for the discount rate: a scenario with government guarantees on low-carbon technology investment (5%), and a scenario of risk aversion toward low-carbon technology investment (12.5%) [75]. A change of ±30% was applied to the O&M costs that correspond to the CSP_{th} Central Tower.

The variable with more influence on the *LCOH* of the CSP_{th} Hybrid-CT system is the capital expenditure, followed by the solar resource, the discount rate, and the O&M costs. Excluding the solar resource, the variables show an apparent linear behavior. For the CSP_{th} Hybrid-CT system (S.M. 1), the *LCOH* is USD 5.21 Cents/kWh_{th}. The 30% reduction in CAPEX produces a *LCOH* of USD 4.66 Cents/kWh_{th}, whereas the 30% increase in this variable produces a *LCOH* of USD 5.76 Cents/kWh_{th}. If the CSP_{th} Hybrid-CT system is designed for a solar resource of 1851 kWh/m^2 (annual DNI), the *LCOH* of the system increases to USD 5.7 Cents/kWh_{th}; on the contrary, if the system is designed for 3576 kWh/m^2 (annual DNI), the *LCOH* falls to 4.89 USD Cents/kWh_{th}. The discount rate of 5% produces a *LCOH* of 4.83 USD Cents/kWh_{th}, whereas the risk-aversion scenario (12.5%) produces a *LCOH* of 5.87 USD Cents/kWh_{th}. The *LCOH* is less sensitive to changes in the O&M costs; a reduction of 30% in this variable produces a *LCOH* of 5.11 USD Cents/kWh_{th}; conversely, an increase of 30% results in USD 5.31 Cents/kWh_{th}. Larger solar multiples extend the effect of the four variables. For example: a 30% reduction in CAPEX lowers the *LCOH* of the CSP_{th} Hybrid-CT system (S.M. 1) by 10.5%; the same reduction lowers the *LCOH* of the CSP_{th} Hybrid-CT system (S.M. 2.5) by 22.6%.

The sensitivity analysis shows that the capital expenditure and the discount rate remarkably affect the LCOH. There is still a high potential to reduce the capital expenditure for this technology [48]. On the other hand, the growing concern about climate change is leading governments, multilateral development banks, and capital funds to stimulate investment in low-carbon technologies through lower costs of capital (discount rates). In this sense, the *LCOH* was calculated with a 20% reduction in the capital expenditure and a discount rate of 5%. The 20% reduction in CAPEX lowers the cost of the three CSP_{th} Hybrid-CT systems (S.M. 2.5 and TES system of 13 h) to 153.52 MMUSD (solar resource: 3576 kWh/m^2), 165.79 MMUSD (solar resource: 2680 kWh/m^2), and 179.12 MMUSD (solar resource: 1851 kWh/m^2). Figure 11 shows the results of this calculation for the CSP_{th} Hybrid-CT systems designed at the three locations.

The main goal of using a CSP_{th} Hybrid-CT system is to reduce both the CO_2 emissions. Considering the power demand of 50 MW_{th}, a fuel-based system produces 106,193 tons of CO_2 per year. Table 8 shows the amount of CO_2 emissions that the CSP_{th} Hybrid-CT systems avoid.

Table 8. Avoided CO_2 emissions per year.

Solar Multiple	Solar Resource (Annual DNI)		
	1851 kWh/m^2	**2680 kWh/m^2**	**3576 kWh/m^2**
1	22,371 tonnes	30,590 tonnes	35,849 tonnes
1.5	35,817 tonnes	48,666 tonnes	57,272 tonnes
2	47,332 tonnes	63,903 tonnes	74,661 tonnes
2.5	58,686 tonnes	78,322 tonnes	88,735 tonnes

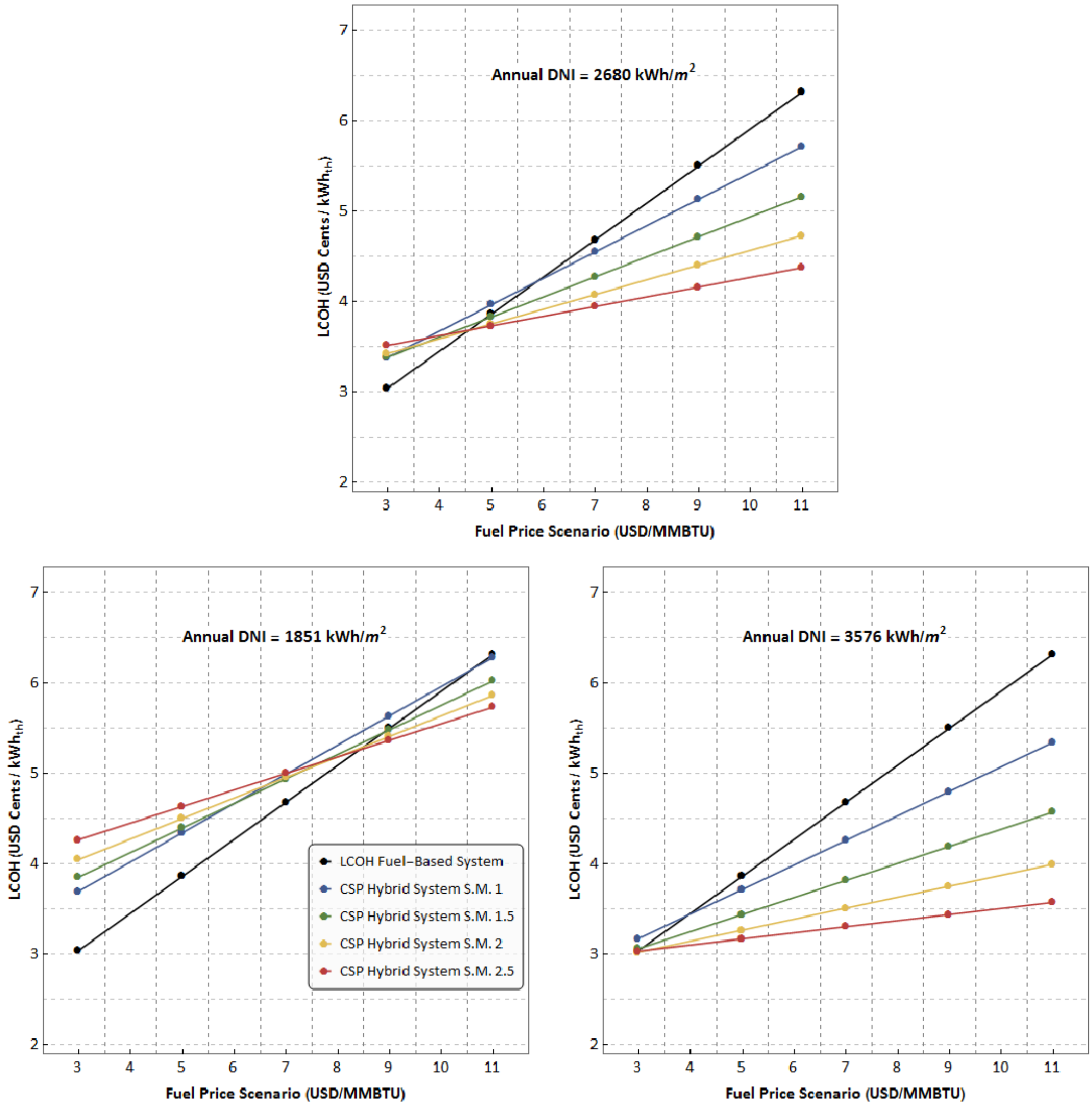

Figure 11. *LCOH* of the CSP_{th} Hybrid-CT systems using a 20% reduction in the capital expenditure and a discount rate of 5%.

The marginal abatement costs were calculated for the three CSP_{th} Hybrid-CT systems designed with a solar multiple of 2.5. As mentioned in Section 2.7, the marginal abatement costs are used as a reference to establish the carbon price needed to trigger abatement measures; for this reason, the *LCOH* values of the CSP_{th} Hybrid-CT systems and the fuel-based system were calculated without pricing the CO_2 emissions. Moreover, the *LCOH* was calculated without any reduction in capital expenditure and using a discount rate of 8%.

Figure 12 shows the marginal abatement costs of these three CSP_{th} Hybrid-CT systems. At the fuel price scenario of 3 USD/MMBTU, the marginal abatement costs are 259, 157, and 115 USD/ton of CO_2 for the systems designed for a solar resource of 1851 kWh/m^2, 2680 kWh/m^2, and 3576 kWh/m^2, respectively. The results show a similar slope for the three systems; the marginal abatement costs decrease 33.6 USD/ton of CO_2 per every increase of 2 USD/MMBTU in the fuel price scenario.

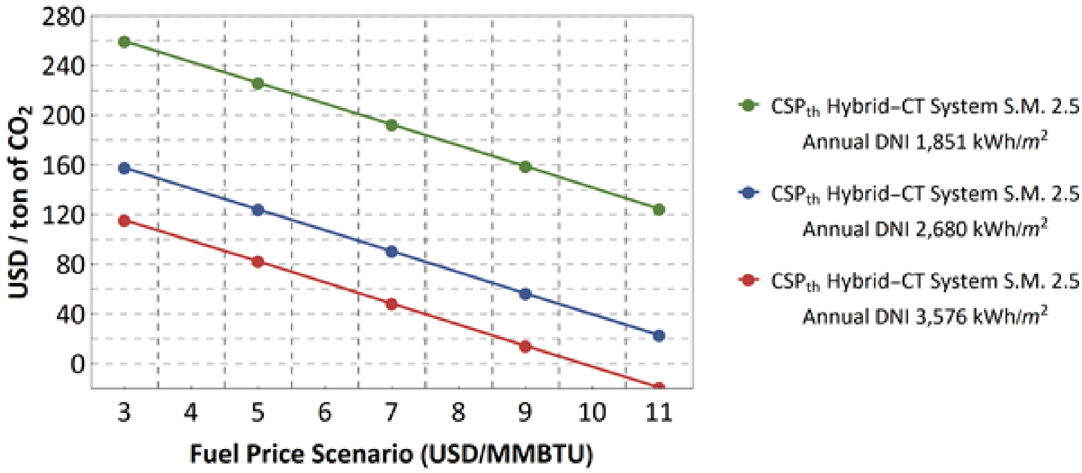

Figure 12. Marginal abatement costs of the CSPth Hybrid-CT systems (S.M. = 2.5).

As shown in Figure 12, the marginal abatement costs of the CSP_{th} Hybrid-CT systems are significantly high at low fuel price scenarios. A CO_2 price of this magnitude compromises the competitiveness of energy consumers [76]; however, if a CO_2 price is not considered, the *LCOH* of these systems is greater than the *LCOH* of fuel-based systems. In this sense, a reasonable CO_2 price should be accompanied by a CAPEX reduction and low costs of capital in order to encourage the deployment of CSP_{th} Hybrid-CT systems as a measure to reduce CO_2 emissions.

5. Conclusions

The CSP_{th} Hybrid-CT technology can produce high-temperature heat for high-temperature industrial processes; this feature makes it a promising option for intensive energy consumers. CSP_{th} Hybrid-CT systems are a high-reliable source of energy and highly effective in avoiding CO_2 emissions compared with fuel-based systems. However, the economic competitiveness of this technology against fuel-based systems depends mainly on two local conditions: the solar resource and fuel prices.

Regarding the *LCOH* of CSP_{th} Hybrid-CT systems, the variables with more influence are the capital expenditure, followed by the solar resource, the discount rate, and the O&M costs. The effect that these variables have on the *LCOH* is extended with solar multiples bigger than 1. In this sense, the study suggests that the capital expenditure and the discount rate are key variables because they create opportunities for cost reductions, especially for large solar multiples, where the heliostat field and the TES system represent a large percentage of the capital expenditure.

In order to effectively deploy CSP_{th} Hybrid-CT systems, CAPEX reductions and low costs of capital should be accompanied with reasonable CO_2 prices. For example: the *LCOH* was calculated considering a 20% reduction in capital expenditure, a discount rate of 5%, and a CO_2 price in line with the recommendations of the High-Level Commission on Carbon Prices. Under these assumptions, the CSP_{th} Hybrid-CT systems show lower *LCOH* than fuel-based systems. For the reference location (annual DNI 2680 kWh/m^2), the *LCOH* of the CSP_{th} Hybrid-CT system (SM 2.5) equals the *LCOH* of a fuel-based system at a fuel price scenario of 4.5 USD/MMBTU; for the other two regions with annual DNIs of 1851 and 3576 kWh/m^2, the breakeven points are 8.5 and 3 USD/MMBTU, respectively.

The *LCOH* values shown in this work result from using two extreme values of solar resource (from 1851 kWh/m^2/year to 3576 kWh/m^2/year) and a medium point (2680 kWh/m^2/year), which was used as the reference case. This provide a valid approximation of the *LCOH* of CSP_{th} Hybrid-CT systems for a significant interval of solar resources, which encompass different regions in the world. In this sense, a wide range of industries might have a notion of the economic competitiveness of this renewable technology against fuel-based systems and which conditions improve this competitiveness. However, in order to have a more accurate perspective, a more detailed study should be conducted in every specific case, including minor and auxiliary components in the analysis.

Author Contributions: Conceptualization, C.A.E.; Methodology, J.M.I.-S.; Research, I.C.-R. All authors participate in writing and editing. All authors have read and agreed to the published version of the manuscript.

Funding: The APC was funded by UNAM-DGAPA-PAPIIT Project No. IG101422.

Acknowledgments: This work was carried out at the Institute of Renewable Energies of the National Autonomous University of Mexico. I.C.-R. thanks CONACYT for the postgraduate scholarship. C.A.E. thanks DGAPA-UNAM for the PAPIIT scholarship for a sabbatical stay at the University of Arizona and for the PAPIIT project IG101422, and J.M.I.-S. thanks the DGAPA-UNAM for the PAPIIT scholarship for a sabbatical stay at the CIEMAT-Spain.

Conflicts of Interest: The authors declare no conflict of interest.

References

1. International Energy Agency. Global Energy & CO2 Status Report: The Latest Trends in Energy and Emissions in 2018. IEA Publications. 2019. Available online: https://www.iea.org/reports/global-energy-co2-status-report-2019/emissions (accessed on 3 November 2022).
2. International Energy Agency. World Energy Outlook 2019. IEA Publications. 2019. Available online: https://www.iea.org/reports/world-energy-outlook-2019 (accessed on 3 November 2022).
3. IRENA/IEA-ETSAP. Solar Heat for Industrial Processes: Technology Brief. IRENA Publications 2015. Available online: https://www.irena.org/Publications (accessed on 3 November 2022).
4. International Energy Agency. Heat Renewables 2019. Available online: https://www.iea.org/reports/renewables-2019/heat (accessed on 3 November 2022).
5. Taibi, E.; Dolf, G.; Morgan, B. *Renewable Energy in Industrial Applications: An Assessment of the 2050 Potential*; United Nations Industrial Development Organization: Vienna, Austria, 2010.
6. Werner, S. ECOHEATCOOL Work Package 1: The European Heat Market. Euroheat & Power. 2006. Available online: https://web.archive.org/web/20130522084453/http://www.euroheat.org/files/filer/ecoheatcool/download.htm (accessed on 3 November 2022).
7. Allouhi, A.; Agrouaz, Y.; Amine, M.B.; Rehman, S.; Buker, M.; Kousksou, T.; Jamil, A.; Benbassou, A. Design optimization of a multi-temperature solar thermal heating system for an industrial process. *Appl. Energy* **2017**, *206*, 382–392. [CrossRef]
8. Quijera, J.A.; Alriols, M.G.; Labidi, J. Integration of a solar thermal system in a dairy process. *Renew. Energy* **2011**, *36*, 1843–1853. [CrossRef]
9. Tschopp, D.; Tian, Z.; Berberich, M.; Fan, J.; Perers, B.; Furbo, S. Large-scale solar thermal systems in leading countries: A review and comparative study of Denmark, China, Germany and Austria. *Appl. Energy* **2020**, *270*, 114997. [CrossRef]
10. Carnevale, E.A.; Ferrari, L.; Paganelli, S. Investigation on the feasibility of integration of high temprature solar energy in a textile factory. *Renew. Energy* **2011**, *36*, 3517–3529. [CrossRef]
11. Sharma, A.K.; Sharma, C.; Mullick, S.C.; Kandpal, T.C. GHG mitigation potential of solar industrial process heating in producing cotton based textiles in India. *J. Clean. Prod.* **2017**, *145*, 74–84. [CrossRef]
12. Bolognese, M.; Viesi, D.; Bartali, R.; Crema, L. Modeling study for low-carbon industrial processes integrating solar thermal technologies. A case study in the Italian Alps: The Felicetti Pasta Factory. *Sol. Energy* **2020**, *208*, 548–558. [CrossRef]
13. Pietruschka, D.; Ben Hassine, I.; Cotrado, M.; Fedrizzi, R.; Cozzini, M. Large Scale Solar Process Heat Systems -planning, Realization and System Operation. *Energy Procedia* **2016**, *91*, 638–649. [CrossRef]
14. Berger, M.; Meyer-Grünefeldt, M.; Krüger, D.; Hennecke, K.; Mokhtar, M.; Zahler, C. First Year of Operational Experience with a Solar Process Steam system for a Pharmaceutical Company in Jordan. *Energy Procedia* **2016**, *91*, 591–600. [CrossRef]
15. Farjana, S.H.; Huda, N.; Mahmud, M.P.; Saidur, R. Solar process heat in industrial systems—A global review. *Renew. Sustain. Energy Rev.* **2018**, *82*, 2270–2286. [CrossRef]
16. Jia, T.; Huang, J.; Li, R.; He, P.; Dai, Y. Status and prospect of solar heat for industrial processes in China. *Renew. Sustain. Energy Rev.* **2018**, *90*, 475–489. [CrossRef]
17. Farjana, S.H.; Huda, N.; Mahmud, M.P.; Saidur, R. Solar industrial process heating systems in operation—Current SHIP plants and future prospects in Australia. *Renew. Sustain. Energy Rev.* **2018**, *91*, 409–419. [CrossRef]
18. Mekhilef, S.; Saidur, R.; Safari, A. A review on solar energy use in industries. *Renew. Sustain. Energy Rev.* **2011**, *15*, 1777–1790. [CrossRef]
19. Kurup, P.; Turchi, C. Initial Investigation into the Potential of CSP Industrial Process Heat for the Southwest United States Initial Investigation into the Potential of CSP Industrial Process Heat for the Southwest United States. 2015. Available online: http:/www.osti.gov/scitech (accessed on 3 November 2022).

20. Joubert, E.; Hess, S.; Van Niekerk, J. Large-scale solar water heating in South Africa: Status, barriers and recommendations. *Renew. Energy* **2016**, *97*, 809–822. [CrossRef]
21. Gabbrielli, R.; Castrataro, P.; Del Medico, F.; Di Palo, M.; Lenzo, B. Levelized Cost of Heat for Linear Fresnel Concentrated Solar Systems. *Energy Procedia* **2014**, *49*, 1340–1349. [CrossRef]
22. Lillo-Bravo, I.; Pérez-Aparicio, E.; Sancho-Caparrini, N.; Silva-Pérez, M.A. Benefits of Medium Temperature Solar Concentration Technologies as Thermal Energy Source of Industrial Processes in Spain. *Energies* **2018**, *11*, 2950. [CrossRef]
23. Sharan, P.; Turchi, C.; Kurup, P. Optimal design of phase change material storage for steam production using annual simulation. *Sol. Energy* **2019**, *185*, 494–507. [CrossRef]
24. Mouaky, A.; Merrouni, A.A.; Laadel, N.E.; Bennouna, E.G. Simulation and experimental validation of a parabolic trough plant for solar thermal applications under the semi-arid climate conditions. *Sol. Energy* **2019**, *194*, 969–985. [CrossRef]
25. McMillan, C.A.; Ruth, M. Using facility-level emissions data to estimate the technical potential of alternative thermal sources to meet industrial heat demand. *Appl. Energy* **2019**, *239*, 1077–1090. [CrossRef]
26. Nathan, G.J.; Jafarian, M.; Dally, B.B.; Saw, W.L.; Ashman, P.J.; Hu, E.; Steinfeld, A. Solar thermal hybrids for combustion power plant: A growing opportunity. *Prog. Energy Combust. Sci.* **2018**, *64*, 4–28. [CrossRef]
27. Schröders, S.; Allelein, H.-J. Energy economic evaluation of process heat supply by solar tower and high temperature reactor based on the ammonia production process. *Appl. Energy* **2018**, *212*, 622–639. [CrossRef]
28. Lawrence Berkeley National Laboratory and Resource Dynamics Corporation. *Improving Process Heating System Performance A Sourcebook for Industry*; The U.S. Department of Energy: Washington, DC, USA, 2015.
29. Sharma, A.K.; Sharma, C.; Mullick, S.C.; Kandpal, T.C. Solar industrial process heating: A review. *Renew. Sustain. Energy Rev.* **2017**, *78*, 124–137. [CrossRef]
30. Hasanbeigi, A.; Harell, G.; Schreck, B. Energy Efficiency Potentials in Industrial Steam Systems in China. Elaborated in Lawrence Berkeley National Laboratory and Published by United Nations Industrial Development Organization. 2014. Available online: https://www.unido.org/researchers/publications (publications database) (accessed on 3 November 2022).
31. Famiglietti, A.; Lecuona-Neumann, A.; Nogueira, J.; Rahjoo, M. Direct solar production of medium temperature hot air for industrial applications in linear concentrating solar collectors using an open Brayton cycle. Viability analysis. *Appl. Therm. Eng.* **2020**, *169*, 114914. [CrossRef]
32. Schoeneberger, C.A.; McMillan, C.A.; Kurup, P.; Akar, S.; Margolis, R.; Masanet, E. Solar for industrial process heat: A review of technologies, analysis approaches, and potential applications in the United States. *Energy* **2020**, *206*, 118083. [CrossRef]
33. Deliotte Consultant. *Impacto Macroeconómico del Sector Solar Termoeléctrico en España*; PROTERMOSOLAR: Sevilla, España, 2011; ISBN 978-84-8198-855-0.
34. He, Y.-L.; Qiu, Y.; Wang, K.; Yuan, F.; Wang, W.-Q.; Li, M.-J.; Guo, J.-Q. Perspective of concentrating solar power. *Energy* **2020**, *198*, 117373. [CrossRef]
35. Téllez Sufrategui, F.M. *Thermal Performance Evaluation of the 200 kWth "SolAir" Volumetric Solar Receiver*; Informes Técnicos; CIEMAT, Plataforma Solar Almeria: Madrid, Spain, 2003.
36. European Commission. *Solgate—Solar Hybrid Gas Turbine Electric Power System*; Office for Official Publications of the European Communities: Luxembourg, 2005; ISBN 92-894-4592-0.
37. Korzynietz, R.; Brioso, J.; del Río, A.; Quero, M.; Gallas, M.; Uhlig, R.; Ebert, M.; Buck, R.; Teraji, D. Solugas—Comprehensive analysis of the solar hybrid Brayton plant. *Sol. Energy* **2016**, *135*, 578–589. [CrossRef]
38. Kumar, L.; Hasanuzzaman, M.; Rahim, N. Global advancement of solar thermal energy technologies for industrial process heat and its future prospects: A review. *Energy Convers. Manag.* **2019**, *195*, 885–908. [CrossRef]
39. Liu, M.; Tay, N.S.; Bell, S.; Belusko, M.; Jacob, R.; Will, G.; Saman, W.; Bruno, F. Review on concentrating solar power plants and new developments in high temperature thermal energy storage technologies. *Renew. Sustain. Energy Rev.* **2016**, *53*, 1411–1432. [CrossRef]
40. Craig, S.; Heat, G.A. *Molten Salt Power Tower Cost Model for the System Advisor Model (SAM)*; Technical Report: NREL/TP-5500-57625; National Renewable Energy Laboratory: Golden, CO, USA, 2013.
41. Turchi, C.S.; Vidal, J.; Bauer, M. Molten salt power towers operating at 600–650 °C: Salt selection and cost benefits. *Sol. Energy* **2018**, *164*, 38–46. [CrossRef]
42. Wagner, M.J.; Wendelin, T. SolarPILOT: A power tower solar field layout and characterization tool. *Sol. Energy* **2018**, *171*, 185–196. [CrossRef]
43. Kolb, G.J. An Evaluation of Possible Next-Generation High-Temperature Molten-Salt Power Towers. Sandia National Laboratories: Albuquerque, NM, USA, 2011.
44. Werner, V.; Henry, K. *Large-Scale Solar Thermal Power: Technologies, Costs, and Development*; © 2010 WILEY-VCH Verlag GmbH & Co. KGaA: Weinheim, Germany, 2010; ISBN 978-3-527-40515-2.
45. National Renewable Energy Laboratory. System Advisor Model: CSP Cost Data. Available online: https://sam.nrel.gov/concentrating-solar-power/csp-cost-data.html (accessed on 3 November 2022).
46. Sargent & Lundy Consulting Group. *Assessment of Parabolic Trough and Power Tower Solar Technology Cost and Performance Forecasts Assessment of Parabolic Trough and Power Tower Solar Technology Cost and Performance Forecasts*; National Renewable Energy Laboratory: Golden, CO, USA, 2003.

47. Pitz-Paall, R.; Dersch, J.; Milow, B. European Concentrated Solar Thermal Road-Mapping. 2005. Available online: https://cordis.europa.eu/project/id/502578/reporting (accessed on 3 November 2022).
48. Kolb, G.J.; Ho, C.K.; Mancini, T.R.; Gary, J.A. *Power Tower Technology Roadmap and Cost Reduction Plan*; Sandia National Laboratories: Albuquerque, NM, USA, 2011. [CrossRef]
49. Hinkley, J.T.; Hayward, J.A.; Curtin, B.; Wonhas, A.; Boyd, R.; Grima, C.; Tadros, A.; Hall, R.; Naicker, K. An analysis of the costs and opportunities for concentrating solar power in Australia. *Renew. Energy* **2013**, *57*, 653–661. [CrossRef]
50. Coelho, B.; Varga, S.; Oliveira, A.; Mendes, A. Optimization of an atmospheric air volumetric central receiver system: Impact of solar multiple, storage capacity and control strategy. *Renew. Energy* **2014**, *63*, 392–401. [CrossRef]
51. Sorbet, F.J.; Iñigo, M.; García-barberena, J.; Bernardos, A. Advanced power cycles and configurations for solar towers: Techno-economical optimization of the decoupled solar combined cycle concept. In Proceedings of the AIP Conference Proceedings, Maharashtra, India, 5–6 July 2018. [CrossRef]
52. Turchi, C.S.; Boyd, M.; Kesseli, D.; Kurup, P.; Mehos, M.; Neises, T.; Sharan, P.; Wagner, M.; Wendelin, T.; Turchi, C.S.; et al. *CSP Systems Analysis—Final Project Report CSP Systems Analysis—Final Project Report*; NREL/TP-5500-72856; National Renewable Energy Laboratory: Golden, CO, USA, 2019.
53. Abaza, M.A.; El-Maghlany, W.M.; Hassab, M.; Abulfotuh, F. 10 MW Concentrated Solar Power (CSP) plant operated by 100% solar energy: Sizing and techno-economic optimization. *Alex. Eng. J.* **2019**, *59*, 39–47. [CrossRef]
54. Hirbodi, K.; Enjavi-Arsanjani, M.; Yaghoubi, M. Techno-economic assessment and environmental impact of concentrating solar power plants in Iran. *Renew. Sustain. Energy Rev.* **2019**, *120*, 109642. [CrossRef]
55. Environmental Protection Agency; International Energy Agency. Boiler Replacement Opportunity. Available online: https://www.epa.gov/sites/default/files/2015-07/documents/fact_sheet_chp_as_a_boiler_replacement_opportunity.pdf (accessed on 3 November 2022).
56. Hernández-Moro, J.; Martínez-Duart, J. Analytical model for solar PV and CSP electricity costs: Present LCOE values and their future evolution. *Renew. Sustain. Energy Rev.* **2013**, *20*, 119–132. [CrossRef]
57. Ren, L.; Zhao, X.; Yu, X.; Zhang, Y. Cost-benefit evolution for concentrated solar power in China. *J. Clean. Prod.* **2018**, *190*, 471–482.
58. Viebahn, P.; Lechon, Y.; Trieb, F. The potential role of concentrated solar power (CSP) in Africa and Europe—A dynamic assessment of technology development, cost development and life cycle inventories until 2050. *Energy Policy* **2011**, *39*, 4420–4430. [CrossRef]
59. Zhu, Z.; Zhang, D.; Mischke, P.; Zhang, X. Electricity generation costs of concentrated solar power technologies in China based on operational plants. *Energy* **2015**, *89*, 65–74. [CrossRef]
60. Sharma, A.K.; Sharma, C.; Mullick, S.C.; Kandpal, T.C. Financial viability of solar industrial process heating and cost of carbon mitigation: A case of dairy industry in India. *Sustain. Energy Technol. Assessments* **2018**, *27*, 1–8. [CrossRef]
61. Zhuang, X.; Xu, X.; Liu, W.; Xu, W. LCOE Analysis of Tower Concentrating Solar Power Plants Using Different Molten-Salts for Thermal Energy Storage in China. *Energies* **2019**, *12*, 1394. [CrossRef]
62. Ji, J.; Tang, H.; Jin, P. Economic potential to develop concentrating solar power in China: A provincial assessment. *Renew. Sustain. Energy Rev.* **2019**, *114*, 109279. [CrossRef]
63. International Energy Agency. Natural Gas Prices for the Industrial Sector. Available online: https://www.iea.org/data-and-statistics/charts/natural-gas-prices-for-the-industrial-sector-in-selected-countries-2019 (accessed on 3 November 2022).
64. U.S. Energy Information Administration. *Annual Energy Outlook 2020 with Projections to 2050*; U.S. Energy Information Administration: Washington, DC, USA, 2020.
65. U.S. Energy Information Administration. Henry Hub Natural Gas Spot Price. Available online: https://www.eia.gov/dnav/ng/hist/rngwhhdA.htm (accessed on 3 November 2022).
66. Carbon Market Watch. Carbon Markets—The Ultimate Guide to Global Offsetting Mechanisms. 2020. Available online: https://carbonmarketwatch.org/publications/carbon-markets-101-the-ultimate-guide-to-global-offsetting-mechanisms/ (accessed on 3 November 2022).
67. ICAP. *Emissions Trading Worldwide: Status Report 2021*; International Carbon Action Partnership: Berlin, Germany, 2021.
68. The World Bank. *State and Trends of Carbon Pricing 2021*; The World Bank: Washington, DC, USA, 2021. [CrossRef]
69. OECD. *Effective Carbon Rates 2018: Pricing Carbon and Emissions Trading*; OECD: Paris, France, 2018.
70. High-Level Commission on Carbon Prices, 2017. Report of the High-Level Commission on Carbon Prices. World Bank Publications. 2018. Washington, DC. Available online: https://www.carbonpricingleadership.org/report-of-the-highlevel-commission-on-carbon-prices (accessed on 3 November 2022).
71. Disclosure Insight Action. Putting a price on carbon: The State of Internal Carbon Pricing by Corporates Globally. 2021. Available online: https://www.cdp.net/en/research/global-reports/putting-a-price-on-carbon (accessed on 3 November 2022).
72. IRENA. *Renewable Energy Options for the Industry Sector: Global and Regional Potential Until 2030*; IRENA Publications: Masdar City, Abu Dhabi, 2015.
73. National Renewable Energy Laboratory. National Solar Radiation Database. Available online: https://nsrdb.nrel.gov/ (accessed on 3 November 2022).
74. Ministerio de Energía, Gobierno de Chile. Explorador Solar. Available online: https://solar.minenergia.cl/ (accessed on 3 November 2022).

75. Carbon Pricing Leadership Coalition. The Carbon Prices Making Low Carbon Plants Competitive. 2017. Available online: https://www.carbonpricingleadership.org/open-for-comments/2017/5/28/the-carbon-prices-making-low-carbon-plants-competitive (accessed on 7 November 2022).
76. World Bank Group. Report of the High-Level Commission on Carbon Pricing and Competitiveness. 2019. World Bank Group, Washington, D.C. Available online: https://www.carbonpricingleadership.org/highlevel-commission-on-carbon-pricing-and-competitiveness (accessed on 7 November 2022).